第33卷第1期
2014年2月

红外与毫米波学报
J. Infrared Millim. Waves

Vol. 33, No. 1
February, 2014

文章编号：1001－9014(2014)01－0019－04

DOI：10.3724/SP.J.1010.2014.00019

Bismuth composition dependence of properties of Bi_xFeO_3 thin films

LI Xiao-Xi[1], DENG Hong-Mei[2], ZHANG Jin-Zhong[1], YANG Ping-Xiong[1]*, CHU Jun-Hao[1]

(1. Key Laboratory of Polar Materials and Devices, Ministry of Education, Department of Electronics, East China Normal University, 500 Dongchuan Road, Shanghai 200241, China;
2. Laboratory for Microstructures, Shanghai University, 99 Shangda Rd, Shanghai 200444, China)

Abstract: The Bi_xFeO_3 films ($0.80 \leqslant x \leqslant 1.20$) were prepared by sol-gel technique on Si substrates. Effects of x variation on microstructures and optical properties of the Bi_xFeO_3 films are reported. It is shown that in the films with both insufficient and excess bismuth dosage, impurity phases such as $Bi_2Fe_4O_9$ and iron oxide appeared. Raman spectra of the films were presented in the spectral range of 50 ~ 800 cm^{-1}. The refractive index (n) of the films decreases with increasing x at wavelength lower than 600 nm, the extinction coefficients (k) of all films were comparable. The bandgaps of the films changed from 2.65 eV to 2.76 eV.

Key words: Bi_xFeO_3 thin film; sol-gel technique; microstructures; optical properties

铋含量的变化对 Bi_xFeO_3 薄膜微结构和光学性质的影响

李晓晞[1]，邓红梅[2]，张金中[1]，杨平雄[1]*，褚君浩[1]

(1. 华东师范大学 极化材料与器件教育部重点实验室，上海 200241；
2. 上海大学 材料研究所 分析测试中心，上海 200444)

摘要：通过溶胶-凝胶技术在Si衬底上制备了x从0.80增大到1.20的Bi_xFeO_3薄膜样品.分析了Bi元素含量的改变对BFO薄膜微结构和光学性质的影响，表明在Bi缺失和Bi过量的Bi_xFeO_3薄膜样品中均出现了$Bi_2Fe_4O_9$杂相和铁氧化物杂相，导致Bi_xFeO_3薄膜晶格的菱形扭曲结构发生变化.测试得到了薄膜的拉曼散射谱和椭圆偏振光谱，拉曼散射谱反映了Bi_xFeO_3薄膜样品中的振动模式明显受到x取值的影响.根据椭偏数据拟合得到的结果表明折射率在波长600 nm以下范围内随着x的减小而减小.而样品的禁带宽度从2.65 eV到2.76 eV，在x为1.05和1.10时得到最大值.

关　键　词：Bi_xFeO_3薄膜；溶胶-凝胶技术；微结构；光学性质

中图分类号：TB303　　**文献标识码**：A

1 Introduction

Multiferroic materials possessing both ferromagnetic and ferroelectric properties simultaneously have attracted enormous attention for their potential applications in multifunctional devices[1] $BiFeO_3$ is a unique multiferroic material for exhibiting both anti-magnetism (T_N ~ 640 K) and strong ferroelectricity (T_C ~ 1 100 K) at room temperature. Therefore a new type of memory device can be expected based on these properties [2].

Nevertheless, researchers have been prevented from obtaining further achievements in application of $BiFeO_3$ by some barriers such as difficulties in produ-

Received date: 2012 - 11 - 12, **revised date**: 2013 - 04 - 18　　**收稿日期**：2012 - 11 - 12，**修回日期**：2013 - 04 - 18

Foundation items: Supported by National Natural Science Foundation of China (60990312 61076060) and Science and Technology Commission of Shanghai Municipality (10JC1404600).

Biography: Li Xiaoxi(1987-), female, East China Normal University, master, research field: ferroelectronics thin film.

* **Corresponding author**: E－mail: pxyang@ee.ecnu.edu.cn.

cing samples with high quality and serious leakage currents of the material [3]. As we all know that the "sol-gel" technique is widely adopted in preparation of $BiFeO_3$ thin films for its high efficiency and practicability. However, experimental environment factors like ambient humidity and annealing atmosphere have great impacts on precursor compounds. A possible solution is to prepare precursors under inert atmospheres which are unlikely to be obtained in most investigations [4] Besides, the volatility of bismuth may also lead to an uncertain proportion among the Bi-Fe-O system in the precursor compounds and further produce a mixture of $BiFeO_3$ and a number of other impurity phases[5-6]. To our knowledge, no bismuth dosage varying precursor solutions have been reported for production of $BiFeO_3$ thin films by sol-gel technique. Hence, we began an extensive study of Bi_xFeO_3 thin films with different value of x to examine its influences on crystallization, microstructure and optical properties of the films.

In this paper, several Bi_xFeO_3 films were prepared via sol-gel technique. The index x in Bi_xFeO_3 thin films varies from 0.80 to 1.20 by changing the molar ratio between $Bi(NO_3)_3 \cdot 5H_2O$ and $Fe(NO_3)_3 \cdot 9H_2O$ while preparing the precursors. The microstructures and properties of multiferroic Bi_xFeO_3 thin films were examined.

2 Experiment

In order to obtain Bi_xFeO_3 thin films with x from 0.80 to 1.20, we adopted $Bi(NO_3)_3 \cdot 5H_2O$ and $Fe(NO_3)_3 \cdot 9H_2O$ as raw materials. These two chemicals were dissolved separately in the mixtures of ethylene glycol and acetic acid and stirred at room temperature for 30 minutes. Then the transparent solutions were mixed together and stirred at room temperature for another hour. The resultant solutions were transparent, blackish red and clear. The process was repeated several times with different $Bi(NO_3)_3 \cdot 5H_2O$ dosages to get Bi_xFeO_3 solutions with different Bi compositions.

The Bi_xFeO_3 thin films were grown by spin coating the obtained precursor solutions on silicon substrates at a low rotating speed of 600 rpm for 5 s, and then high speed of 4 000 rpm for 20 s. Films were pre-fired at 350 ℃ for 3 minutes and annealed at 650 ℃ for 4 minutes in air to be well crystallized. These processes were repeated six times for each sample to obtain the film of desired thickness.

The structural properties of the samples were examined by x-ray diffraction (XRD). Raman spectra were exploited by a micro-Raman spectrometer with the wavelength ranging from 50 cm^{-1} to 800 cm^{-1}. The influences of the different Bi composition on the extinction coefficient and refractive index were investigated using spectroscopic ellipsometry.

3 Results and discussion

The effects of Bi cation ratio variation on the crystalline phase and structure of the Bi_xFeO_3 thin films were identified by XRD analysis. Figure 1 shows the XRD patterns of Bi_xFeO_3 thin films. The results represent that only when x = 1.00, the sample consists of pure perovskite BFO phase without any peaks indicating secondary phases. For all the rest stoichiometries, peaks for orthorhombic $Bi_2Fe_4O_9$ appeared. Even for the widely used stoichiometry of 1.05[7], there is a weak peak at around 29.3 degree representing $Bi_2Fe_4O_9$ phase. This demonstrates the difficulty of forming single phase $Bi_2Fe_4O_9$ thin films. When Bi cation ratios fall below 1, these samples appear to be a mixture of at least three phases, which are BFO, orthorhombic $Bi_2Fe_4O_9$ and a third phase believed to be the iron oxide of $Fe_{0.902}O$, as shown in Figure 1. This indicates the phase formation towards the Bi-deficient phases

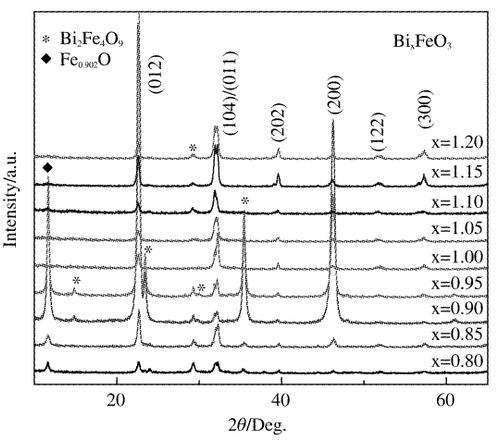

Fig. 1 XRD patterns of the Bi_xFeO_3 films on Si substrates

图1 硅衬底上生长的 Bi_xFeO_3 薄膜的X射线衍射图

with the Bi content decreasing. Especially, the intensity ratio of the doubly split peaks (104) to (011) in the ranges of 31 ~ 33° tends toward one with the value of index x deviating away from 1.00. Similar changes were also observed in the XRD patterns of Nd-doped $BiFeO_3$ ceramics[8] and mutiferroic $BiFeO_3$ bulk ceramics with various sintering temperatures[9]. It can be attributed to a phase transformation towards a nonrhombohedral symmetry or a change in the rhombohedral distortion with bismuth content reaching towards both extremes.

Microstructure and surface morphology of the Bi_xFeO_3 thin films were characterized by AFM. Figure 2 shows the three dimensional and surface micrographs of the Bi_xFeO_3 thin films with x at 0.95 and 1.05, respectively. As can been seen in figure 2, the surface morphology presents different patterns with various values of the index x. The surface of the film with x at 1.05 is denser, indicating few voids. The root mean square roughnesses of different samples were calculated. The RMS roughness of x = 0.95 sample is 9.48 nm. It dramatically falls down to 2.58 nm with x increasing to 1.05. The large variation can obviously affect the lattice vibrations and optical properties of the films, such as second-order Raman-active frequencies, high frequency dielectric constants, and optical band gap, which will be discussed later.

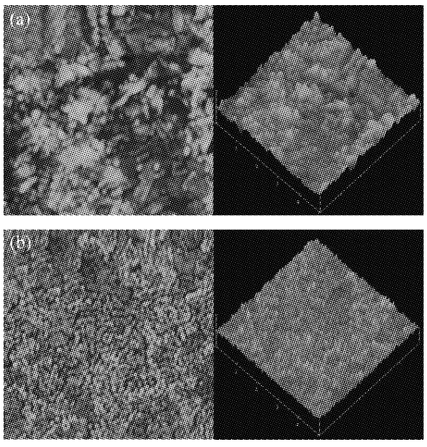

Fig. 2　AFM surfaces and three dimensional micrographs of the Bi_xFeO_3 films with x at 0.95 and 1.05, respectively

图 2　(a) x 为 0.95 (b) x 为 1.05 时的 Bi_xFeO_3 薄膜 AFM 形貌图

Figure 3 shows the room-temperature unpolarized Raman spectra of Bi_xFeO_3 thin films on Si substrates. The room-temperature crystal structure of Bi_xFeO_3 is a highly rhombohedrally distorted perovskite, which belongs to space group R3c. The selection rules for the Raman active modes in rhombohedral R3c symmetry predict only 13 active Raman phonons with A_1 and E symmetries, according to the irreducible representation, $\Gamma_{Raman/IR} = 4A_1 + 9E$. Most of the Raman studies have focused in the frequency range below ~ 700 cm^{-1} since all these modes fall in this region [10]. Herein, we present Raman spectra in the 50 ~ 800 cm^{-1} spectral range.

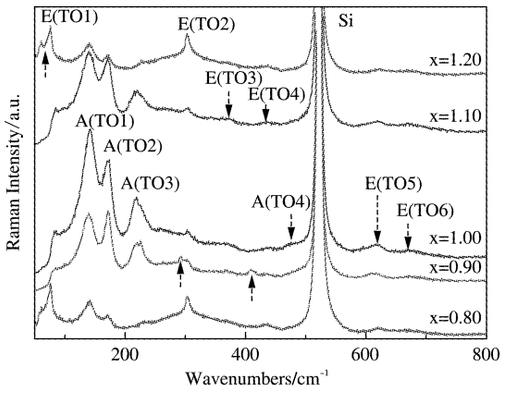

Fig. 3　Room-temperature unpolarized Raman spectra of the Bi_xFeO_3 films on Si substrate

图 3　室温下硅衬底上生长的 Bi_xFeO_3 薄膜拉曼散射谱

The spectra show strong peaks at around 76, 84, 141, 172, 219, 302, 437 and 621 cm^{-1}, and comparatively weak peaks at around 98, 261, 371, 473 and 675 cm^{-1}, as shown in figure 3. By comparing with previously reported data [11-14], the strong peaks at 141, 172, 219, and a weak peak at 473 cm^{-1} can be assigned to the $4A_1$ modes and the remaining peaks are assigned to the E modes. However, some additional peaks, such as the one around 62 cm^{-1} in x of 0.8 and 1.20 samples and 293 cm^{-1} in x of 0.9 sample, are difficult to assign since their origins are not fully understood, but it is possible that they are caused by scattering from the impurity phases or second-order scattering feature.

A further observation of individual peaks exposits that a significant difference in the peak intensity and

width among the samples, all three A_1 modes in low-frequency range become hardened as the index x increases when $x < 1.0$, and they become weakened when $x > 1.0$. It has been reported in previous work that Bi atoms only participate in low-frequency modes up to 167 cm^{-1}, while Fe atoms are mainly involved in modes between 152 and 261 cm^{-1} but also contribute to some higher-frequency modes[15]. Thus the observed variation of A_1 modes can be generally attributed to the changing of both Bi-O and Fe-O covalent bonds.

Additionally, the E_1 peak at 84 cm^{-1} in the sample x of 1.00 and 1.10 disappeared in other samples, substituted by a new rising peak around 76 cm^{-1}, which also represents an E mode for Bi_xFeO_3. This discrepancy can tentatively be correlated with the results obtained from the XRD result that a phase transformation towards a nonrhombohedral symmetry or a change in the rhombohedral distortion occurred.

Ellipsometric spectra are collected with a spectral range from 400 to 1 000 nm. Figure 4 shows the refractive indexes n and the extinction coefficients k of the films, respectively. As shown in the figure 4a, the plots of the refractive index rise towards short wavelength, showing the typical shape of a dispersion curve. The refractive index decreases with x in wavelength lower than 600 nm except for x of 0.85. From the figure 4b, it is found that the extinction coefficients of all films were comparable, while k is slightly higher in x = 1.15 sample at the wavelength around 500 nm.

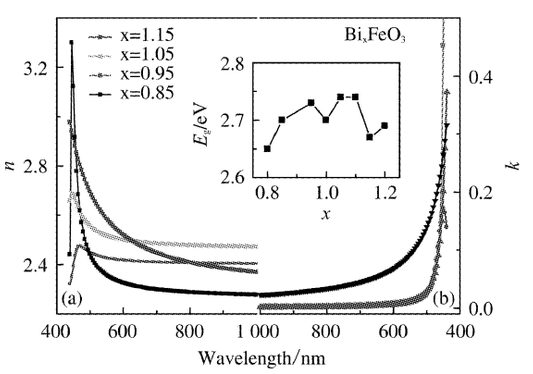

Fig. 4 The refractive indexes n (a) and the extinction coefficients k (b) of the Bi_xFeO_3 films, respectively. Inset shows the bandgaps of the Bi_xFeO_3 films

图4 Bi_xFeO_3 薄膜的(a)折射率(b)消光系数. 插图所示的是 Bi_xFeO_3 薄膜的禁带宽度

Moreover, we can obtain bandgaps of the Bi_xFeO_3 films from the ellipsometric spectra[16], as shown in the inset of figure 4. With x increa sing from 0.80 to 1.20, the bandgaps first increase from 2.65 eV to 2.76 eV before x reaches 1.10, and then begin to fall down. This variation is possibly caused by the impurity phases such as orthorhombic $Bi_2Fe_4O_9$ which appear in both samples with insufficient and excess bismuth dosage

4 Conclusions

In summary, the Bi_xFeO_3 ($0.80 \leqslant x \leqslant 1.20$) films were grown on Si substrates. The effects of the variation of the Bi content on the microstructure and optical properties of the Bi_xFeO_3 films were discussed. It is clear that the impurity phases such as orthorhombic $Bi_2Fe_4O_9$ is induced by both insufficient and excess bismuth dosage and changes the properties of the Bi_xFeO_3 films.

Acknowledgements

This work was supported by the National Natural Science Foundation of China (No. 60990312 and No. 61076060), and Science and Technology Commission of Shanghai Municipality (10JC1404600).

REFERENCES

[1] Ramesh R, Spaldin NA. Multiferroics: progress and prospects in thin films[J]. *Nature Materials* 2007;**6**: 21-29.

[2] Singh SK, Shanthy S, Ishiwara H. Reduced leakage current in $BiFeO_3$ - $BiCrO_3$ nanocomposite films formed by chemical solution deposition [J]. *J Appl Phys* 2010; **108**: 054102.

[3] Eerenstein W, Mathur ND, Scott JF. Multiferroic and magnetoelectric materials. [J]. *Natural* 2006;**442**: 759-765.

[4] Boyle TJ, Buchheit CD, Rodriguez MA, Al-Shareef HN, Hernandez BA. Formation of SrBi2Ta2O9: Part I, Synthesis and Characterization of a Novel Sol - Gel Solution for Production of Ferroelectric SrBi2Ta2O9 Thin Films[J]. *J Mater Res* 1996;**11**: 2274-2281.

[5] Kim JK, Kim SS, Kim WJ. Sol-Gel Synthesis and Properties of. Multiferroic $BiFeO_3$ [J]. *Mater Lett* 2005; **59**: 4006-4009.

[6] Singh SK, Funakuba H, Uchida H, Ishiwara H. Structural and electrical properties of BiFeO3 thin films[J]. *Integrated Ferroelectrics* 2005;**76**: 139-146.

[7] Huang FZ, Lu XM, Lin WW, *et al*. Thickness-dependent structural and magnetic properties of BiFeO films prepared by metal organic decomposition method[J]. *Appl Phys Lett* 2010;**97**: 222901.

(下转第35页)

As the ADN content decreases, the visible EL intensity decreases largely. Compared with the 5∶1 device, the visible EL intensity for the 1∶1 device decreases by 60 times and that for the 1∶5 device is too weak to be detected and is referred as the background line. The fact that ErQ reduces the visible EL of the ADN indicates that the energy transfer from ADN to ErQ occurs.

3 Conclusion

We demonstrated the 1.54 μm EL from Si-OLEDs with the ErQ/ADN bilayer, (ErQ/ADN) ×3 multilayer, and ErQ: ADN doped layer with varying doping levels, among which the 1∶1 doped structure is the most efficient one in 1.54 μm EL. High-efficiency intersystem energy transfer between Er complex and ADN is responsible for the efficient 1.54 μm EL.

REFERENCES

[1] Zang F X, Li W L, Hong Z R, *et al.* Observation of 1.5 μm photoluminescence and electroluminescence from a holmium organic complex[J]. *Applied Physics Letters*, 2004, **84**(25): 5115-5117.

[2] Izeddin I, Moskalenko A S, Yassievich I N, *et al.* Nanosecond dynamics of the near-infrared photoluminescence of Er-doped SiO2 sensitized with Si nanocrystals[J]. *Physical Review Letters*, 2006, **97**(20).

[3] Harrison B S, Foley T J, Bouguettaya M, *et al.* Near-infrared electroluminescence from conjugated polymer/lanthanide porphyrin blends[J]. *Applied Physics Letters*, 2001, **79**(23): 3770-3772.

[4] Gillin W P, Curry R J. Erbium (III) tris(8-hydroxyquinoline) (ErQ): A potential material for silicon compatible 1.5μm emitters[J]. *Applied Physics Letters*, 1999, **74**(6): 798-799.

[5] Zhao W Q, Wang P F, Ran G Z, *et al.* 1.54 μm Er3+ electroluminescence from an erbium-compound-doped organic light emitting diode with a p-type silicon anode[J]. *Journal of Physics D-Applied Physics*, 2006, **39**(13): 2711-2714.

[6] Wei F, Li Y Z, Ran G Z, *et al.* 1.54 μm electroluminescence from p-Si anode organic light emitting diode with Bphen: Er(DBM)(3)phen as emitter and Bphen as electron transport material[J]. *Optics Express*, 2010, **18**(13): 13542-13546.

[7] Kum Hee L, Jae Nam Y, Sunwoo K, *et al.* Synthesis and electroluminescent properties of blue-emitting t-butylated bis(diarylaminoaryl) anthracenes for OLEDs[J]. *Thin Solid Films*, 2010, **518**(22): 6253-6258.

[8] Li-Ning S, Hong-Jie Z, Lian-She F, *et al.* A new sol-gel material doped with an erbium complex and its potential optical-amplification application[J]. Advanced Functional Materials, 2005, **15**(6): 1041-1048.

[9] Hao T, Xiuru W, Ying L, et al. Green organic light-emitting diodes with improved stability and efficiency utilizing a wide band gap material as the host[J]. Displays, 2008, **29**(5): 502-505.

[10] Park Y-S, Jeong W-I, Kim J-J. Energy transfer from exciplexes to dopants and its effect on efficiency of organic light-emitting diodes[J]. Journal of Applied Physics, 2011, **110**(12).

(上接 22 页)

[8] Yuan GL, Or SW, Liu JM, *et al.* Structural transformation and ferroelectromagnetic behavior in single-phase BiNdFeO multiferroic ceramics[J]. *Appl Phys Lett* 2006;**89**: 052905.

[9] Rout D, Moon KS, Kang SJL. Temperature-dependent Raman scattering studies of polycrystalline BiFeO3 bulk ceramics[J]. *J Raman Spectrosc* 2009;**40**: 618-626.

[10] Ramirez MO, Krishnamurthi M, Denev S, *et al.* Magnon sidebands and spin-charge coupling in bismuth ferrite probed by nonlinear optical spectroscopy[J]. *Appl Phys Lett* 2008;**92**: 022511.

[11] Fukumura H, Harima H, Kisoda K, *et al.* Raman and infrared spectra of multiferroic bismuth ferrite from first principles[J]. *J Magn Magn Mater* 2007;**310**: e367-9.

[12] Singh MK, Jang HM, Ryu S, *et al.* Polarized Raman scattering of multiferroic BiFeO epitaxial films with rhombohedral R3c symmetry[J]. *Appl Phys Lett* 2006;**88**: 042907.

[13] Cazayous M, Malka D. Electric field effect on BiFeO3 single crystal investigated by Raman spectroscopy[J]. *Appl Phys Lett* 2007;**91**: 071910.

[14] Kothari D, Reddy VR, Sathe VG, *et al.* Raman scattering study of polycrystalline magnetoelectric BiFeO3[J]. *J Magn Magn Mater* 2008;**320**: 548-552.

[15] Hermet P, Goffinet M, Kreisel J, Raman and infrared spectra of multiferroic bismuth ferrite from first principles[J]. *Phys Rev B* 2007;**75**: 220102.

[16] Yang PX, Guo M, Shi MR. Spectroscopic ellipsometry of SrBiTaNbO ferroelectric thin films[J]. *J Appl Phys* 2005; **97**: 106106.